One test to predict them all: Rheological characterization of complex fluids via artificial neural network

(article starts on next page)

Contents lists available at ScienceDirect

Engineering Applications of Artificial Intelligence

One test to predict them all: Rheological characterization of complex fluids via artificial neural network

Ases Akas Mishra [a],*, Viney Ghai [a], Valentina Matovic [a], Dragana Arlov [b], Roland Kádár [a],*

[a] *Chalmers University of Technology, Department of Industrial and Materials Science, Göteborg, 41296, Sweden*
[b] *Tetra Pak Processing Systems, Lund, 22186, Sweden*

ARTICLE INFO

ABSTRACT

The rheological behavior of complex fluids, including thixotropy, viscoelasticity, and viscoplasticity, poses significant challenges in both measurement and prediction due to the transient nature of their stress responses. This study introduces an artificial neural network (ANN) designed to digitally characterize the rheology of complex fluids with unprecedented accuracy. By employing a data-driven approach, the ANN is trained using transient rheological tests with step inputs of shear rate. Once trained, the network adeptly captures the intricate dependencies of rheological properties on time and shear, enabling rapid and accurate predictions of various rheological tests. In contrast, traditional phenomenological structural kinetic constitutive models often fail to accurately describe the evolution of nonlinear rheological properties, particularly as material complexity increases. The ANN demonstrates high flexibility, reliability and robustness by accurately predicting transient rheology of varied materials with different shear histories. Our findings illustrate that ANNs can not only complement and validate traditional rheological characterization methods but also potentially replace them, thereby paving the way for more efficient material development and testing.

1. Introduction

Robust and reliable prediction of rheological properties of soft matter is essential for its production, processing and utility in various applications (Salehi et al., 2023; Tucker, 2017; Mishra et al., 2022). One of the greatest challenges in this respect arises from a time-dependent complex material structure imparting transient characteristics to the material. In particular, thixotropy is a topic of ongoing substantial interest (Bhattacharyya et al., 2023; Choi et al., 2021), with many fundamental challenges on understanding the nature thereof still remaining. In thixotropic fluids, structural agglomerates can be broken down by the application of a shear stress/shear rate for finite amount of time. After the cessation of shear, the microstructure will intrinsically tend towards its thermodynamic equilibrium state under the influence of rotational Brownian motion, resulting in microstructural recovery. While shear-induced structural breakdown can be achieved within very short timescales, for thixotropic fluids complete microstructural recovery happens over an extensive timescale (at rest), i.e. several hours, and therefore beyond the timescale of most rheological/flow experiments (Nijenhuis et al., 2007). In most cases, thixotropy manifests itself along with yield stress and both properties originate from the same basic physics (Møller et al., 2006). Yield stress is the critical stress required to induce viscoplastic deformation or flow. For simple

yield stress fluids there is only a shear rate dependency which makes it easier to find a sharp yield stress point. Whereas, for thixotropic yield stress fluids, there is an additional time dependency, making it difficult to measure yield stress and obtain repeatable results (Bauer and Collins, 1967; Barnes, 1997; Mewis and Wagner, 2009). Furthermore, most complex fluids are viscoelastic, exhibiting both elastic and viscous behavior under deformation. The amalgamation of non-linear and transient material properties make the study, testing and prediction of time dependent materials challenging.

Numerous structural kinetic models (SKMs) have been proposed to model the transient behavior of thixo-elasto-viscoplastic (TEVP) soft matter (Mewis and Wagner, 2009; Toorman, 1997; Dullaert and Mewis, 2006; Pinder, 1964; Bénézech and Maingonnat, 1993). SKMs consist of kinetic equations that model the time dependency of the structure of the fluid and an equation of state that relates the structural evolution to the shear stress or viscosity. As material complexity increases, higher number of model parameters are required to predict rheological properties. Conventional curve fitting and modeling approaches to obtain model parameters are time consuming and become increasingly difficult when dealing with models such as the IKH (Wei et al., 2018) and ML-IKH (Dimitriou and McKinley, 2014), which contain up to

13 parameters, only some of which can be determined from experiments while others need to be extracted from curve fitting to different rheological experiments (Larson and Wei, 2019).

Artificial neural network (ANN) architectures have exponentially improved predictive capabilities across various scientific disciplines (Taherdoost, 2023; Abdelsalam et al., 2024b,a, 2025; Ghania et al., 2024). ANN assisted rheological characterization has great potential for process optimization, quality control, or material design in industrial applications. The use of ANN models to predict rheology has been of great interest recently. Mahmoudabadbozchelou et al. used a physics-informed neural network (PINN) to predict viscoelastic rheological properties of fumed silica suspension using the Maxwell-IKH model (Mahmoudabadbozchelou et al., 2022). In another study by the same group, ANN was used to construct a constitutive mathematical model from scratch using a data driven approach (Mahmoudabadbozchelou et al., 2024). Similarly, a few other studies have used SKMs and data driven approaches to predict complex rheological properties using neural networks (Nagrani et al., 2023; Mahmoudabadbozchelou and Jamali, 2021; Zhang et al., 2023). When dealing with transient material behavior, traditional constitutive models face substantial challenges, particularly as material complexity grows and introduces non-monotonic effects on transient data. ANN present a promising approach to address these complexities, offering unprecedented predictive accuracy and robustness in modeling intricate material behaviors. PINNs integrate governing physical laws into the training process, enhancing prediction realism and ensuring adherence to fundamental principles. However, they can be complex to implement, requiring substantial computational resources and extensive hyperparameter tuning. In contrast, data-driven neural networks offer flexibility and robustness, relying solely on available data for pattern learning. This approach excels with rich datasets and is easier to implement, though it faces challenges like overfitting and data quality dependence. Given the context of this research, the choice of a data-driven approach is justified by the availability of extensive datasets and the need for adaptable models.

When it comes to predicting the next value in a time series, ANN models must make single-step-ahead predictions without allowing the anticipated value to influence the input regressor. However, for more complex, long-term predictions, the output must be fed back into the input regressor for a set number of time steps. As a result, the input regressor gradually shifts from containing actual sample points to incorporating previously predicted values (Menezes and Barreto, 2008). As the prediction horizon extends towards infinity, a time series model is required to estimate future values of the input regressor. Eventually, the input regressor comprises solely estimated values of the time series, thereby transforming the multi-step-ahead prediction task into a dynamic modeling endeavor. This transition necessitates the use of advanced modeling techniques to achieve accurate predictions (Menezes and Barreto, 2008). It is widely recognized that the tasks of multi-step-ahead prediction and dynamic modeling entail markedly greater complexity compared to their single-step-ahead prediction counterparts. Recurrent neural architectures, in particular, have been shown to be heavily relied upon in the context of these tasks. The utilization of recurrence architectures has been widely discussed in the literature, particularly in the context of training these architectures using temporal gradient-based variations of the backpropagation algorithm (Pearlmutter, 1995). The task of mastering temporal dependencies across extended intervals in input–output signals can present significant challenges when utilizing gradient-based learning algorithms. It has been previously shown that the utilization of gradient-descent methodologies for acquiring prolonged temporal dependencies proves to be more effective in a specific category of simple recurrent network model called Nonlinear Autoregressive with eXogenous input (NARX), as compared to traditional recurrent models (Menezes and Barreto, 2008; Lin et al., 1998).

In this study, we demonstrate the capabilities of NARX ANN to predict the non-monotonic, transient rheological behavior of TEVP fluids. We use yogurt as a test fluid, which along with other food products constitute some of the most difficult material responses to measure and predict (Amini et al., 2024; Ramaswamy and Basak, 1991; Prajapati et al., 2016; Benezech and Maingonnat, 1994; Abu-Jdayil and Mohameed, 2002). It is made through a fermentation process that involves milk, specific types of bacteria and a significant number of volatile compounds during fermentation (Chen et al., 2017). The aggregation of caesin and formation of a three dimensional (percolated) denatured (low pH) protein structure imparts TEVP rheological functions to the material. We show that a data-driven ANN model that does not rely on constitutive rheological equations (e.g. SKMs), trained on a transient rheological experiment, is capable of predicting TEVP properties of the material. The predictive accuracy of the ANN surpasses all SKMs and least-squared curve fitting methods in forecasting transient rheological properties. The ANN gains temporal context by training on data from a simple step change in shear rate test, learning the intricate dependence of transient shear stress response on shear history. While constitutive models with numerous fit parameters are difficult to fit and implement as non-unique combinations of model constants can satisfy the fit, the data-driven ANN approach enables quick and accurate digital rheological characterization of complex fluids once trained on transient tests.

2. Materials and experimental procedures

2.1. Materials

Three types of yogurt samples, a standard stirred yogurt, a stirred yogurt containing flavor additives and a yogurt produced by fermentation using a different bacteria culture (Boosjin et al., 2016) and with higher fat content were investigated (see Table S1 in supplementary information). The yogurts chosen for this study (Arla Foods, Viby, Denmark) are Naturell, Vanilj, and Långfil, designated as N, V, and L respectively in this paper. These are typical varieties found in the Swedish and Danish markets. Samples were purchased off-the-shelf and stored at 2 °C. Newly bought samples were used for all experiments, well within their expiry dates to ensure their freshness and reduce measurement errors due to bacterial growth.

2.2. Rheological characterization

Rheological measurements were performed on an Anton Paar MCR702e Space rheometer (Graz, Austria) using a profiled bob and cup measuring geometry (CC27/P6), inner diameter of cup being 29 mm and outer diameter of bob being 27 mm. The measurements were performed in single motor-transducer configuration. The C-ETD 200/XL accessory was used to maintain the measuring temperature constant at 23 °C. The yogurt samples were removed from the refrigerator 30 min before each measurement to allow the sample to naturally warm up to the room temperature (23 °C). For each measurement, 20 ml of the sample was gently poured into the measuring cup and the bob was slowly moved down to the measuring position to avoid unwanted structure break-up. The sample was then allowed to rest for 5 min before starting the experiments.

A step change in shear rate experiment, also known as Multi Interval Thixotropy (MITT) test, consist of successive shear rate step inputs and captures structural breakdown and recovery in response to sudden changes in shear levels. 8 arbitrary intervals of 120 s each, with different input shear rates were applied and the resulting shear stress response was measured. The input shear rates were chosen in such a way that the corresponding shear stresses were above and below the yield stress of the material. This was necessary to capture both structural breakdown and buildup of the sample. After preliminary

tests, MITT data was used to train the neural network and fit the SKMs to extract model parameters.

To measure thixotropy, hysteresis loop tests were performed. A shear rate ramp up in the range of $\dot{\gamma} \in [10^0, 10^3]$ s^{-1} and subsequent ramp down from $[10^3, 10^0]$ s^{-1} was imposed, with a constant time step size of 120 s for each shear rate step. The hysteresis loop tests were performed in triplicates to minimize measurement errors and ensure repeatability. Oscillatory shear strain sweep measurements were performed to assess viscoelasticity of the test samples. Dynamic moduli (G' and G'') were measured in strain sweep tests in the strain amplitude range of $\gamma_0 \in [10^{-2}, 10^2]$% at a constant angular frequency of 6 rad/s. Stress controlled steady shear tests were performed to determine static yield stress (σ_y). Shear stress ramp between $\sigma \in [10^0, 10^2]$ Pa was imposed and shear viscosity (η) was measured. When applied stress exceeds the yield stress of the material, viscosity decreases as the material transitions from elastic to plastic deformation and subsequently starts to flow. Intersection of tangents drawn on the two slopes gives σ_y. The yield stress range was measured with creep tests, wherein the transient shear viscosity (η^+) evolves as function of time and imposed constant shear stress. When a stress greater than the yield stress of the material is applied, the structure breaks down, causing a decrease in η^+. When the applied stress is smaller than the yield stress of the material, structural recovery results in an increase of η^+. However, when the imposed stress is within the yield stress range of the material, structural breakdown and recovery compete and η^+ fluctuates before achieving steady or quasi-steady state. Creep tests reveal structural dynamics of the fluid and are also used to estimate the time required to achieve steady state (Coussot et al., 2002b).

2.2.1. Morphological characterization

The morphology of yogurts was analyzed using a Phillips XL-30 (Amsterdam, Netherlands) environmental scanning electron microscope (ESEM). To probe the structural dynamics of yogurt, samples were extracted from the cup geometry with a spatula and the sample morphology was arrested at given experimental times using liquid nitrogen, followed by freeze-drying for 72 h. A small piece of freeze-dried sample was mounted onto a stub covered with carbon tape. The sample was then sprayed with 5 nm gold in a vacuum sputter to enhance conductivity and reduce electrostatic discharging. SEM images were further analyzed using Fiji (Schindelin et al., 2012) to evaluate the yogurts' network connectivity. The images were first binarized and then processed using the Skeletonize plugin to reduce the binary images into network maps through surface/axis thinning algorithms (Lee et al., 1994).

2.3. Structural kinetic modeling

Three different SKMs are considered for comparative analysis. To model the thixotropy of a material, a structural parameter, $\lambda(t)$, is introduced in the formulation of viscosity through an equation of state (EOS). $\lambda(t)$ varies from 0 to 1 and quantifies the level of structure present in the material: $\lambda(t) = 0$ represents complete breakdown of the structure and $\lambda(t) = 1$ represents complete buildup. The time dependence of the structural parameter is then given by a kinetic or rate equation. A large variety of EOSs of varying complexity have been proposed in the scientific literature (Mewis and Wagner, 2009; Mujumdar et al., 2002). Based on heuristic arguments (Fazilati et al., 2021), we chose an EOS of the form

$$\eta(\lambda(t), \dot{\gamma}) = [K_1 + K_2\lambda(t)]\dot{\gamma}^{m-1} \tag{1}$$

coupled to a generalized kinetic equation of the form

$$\frac{d\lambda(t)}{dt} = \underbrace{k_1\dot{\gamma}^a\lambda(t)^b}_{\text{Breakdown}} + \underbrace{k_2\dot{\gamma}^c(1-\lambda(t))^d}_{\text{Buildup}}. \tag{2}$$

K_1, K_2, the power law index m in Eq. (1) and k_1, k_2 in Eq. (2) are model coefficients to be determined. The EOS considers the instantaneous

Table 1
Summary of SKMs consisting of an equation of state and kinetic equation used in the study. The generalized form of the kinetic equation can be found in Eq. (2).

Equation of State (EOS)	Author & Indices, Eq. (2)	Kinetic equation
$\sigma = [K_1 + K_2\lambda(t)]\dot{\gamma}^m$	Mujumdar et al. (2002) $a = 1,\ b = 1,\ c = 0,\ d = 1$	$\frac{d\lambda(t)}{dt} = -k_1\dot{\gamma}\lambda(t) + k_2[1 - \lambda(t)]$
	Worrall and Tuliani (1964) $a = 1,\ b = 1,\ c = 1,\ d = 0$	$\frac{d\lambda(t)}{dt} = -k_1\dot{\gamma}\lambda(t) + k_2\dot{\gamma}$
	Coussot et al. (2002a) $a = 1,\ b = 1,\ c = 0,\ d = 0$	$\frac{d\lambda(t)}{dt} = -k_1\dot{\gamma}\lambda(t) + k_2$

shear rate dependence of the viscosity through a power law component and thixotropic effects through the structural parameter. Alternatively, Eq. (1) can be expressed in terms of the shear stress,

$$\sigma(\lambda(t), \dot{\gamma}) = [K_1 + K_2\lambda(t)]\dot{\gamma}^m \tag{3}$$

Structural breakdown in Eq. (2) is represented by the first term on the right hand side and the structural buildup by the second term. Indices a, b, c and d, essentially define the three kinetic equations investigated in this study, i.e. by Mujumdar et al. (2002), Worrall and Tuliani (1964) and Coussot et al. (2002b), see the overview in Table 1.

Using a custom MATLAB code for curve fitting the SKMs, the least squared error between experimental and simulated shear stress response was minimized to extract the values of the model parameters k_1, k_2, K_1, K_2 and m. The EOS and kinetic equation were simultaneously solved to obtain the shear stress. Thereafter, the complete model with its fitted coefficients was used to predict other rheological curves.

2.4. NARX neural network

The NARX neural network is a dynamic neural structure that has been widely used for input–output modeling of deterministic non-linear dynamic systems. When applied to the prediction of time series data, the NARX network is typically designed as a Feed Forward Time Delay Neural Network (TDNN). A simplified structure of the NARX ANN is presented in Fig. 1. The NARX model can be mathematically represented as follows-

$$\hat{y}(t) = f[u(t), u(t-1), \dots, u(t-n_u), y(t-1), \dots, y(t-n_y)] + e_t \tag{4}$$

The model consists of target and predicted variables, $y(t)$ and $\hat{y}(t)$ respectively. The model prediction of the next value of $\hat{y}(t)$ is regressed on its previous value and an exogenous input variable, $u(t)$. n_u and n_y are the time delays (D) of the input and output variables and $e(t)$ is the error between the predicted and target values. The hidden layer output at time t is $H_i(t)$ and is given by the hidden layer activation function $f_1(\cdot)$-

$$H_i(t) = f_1\left[\sum_{r=0}^{n_u} w_{ir}u(t-r) + \sum_{l=1}^{n_y} w_{il}y(t-l) + a_i\right] \tag{5}$$

where w_{ir} is the weight of the connection between the input neuron $u(t-r)$ and the ith hidden neuron. Whereas, w_{il} is the weight between the ith hidden neuron and the output feedback neuron $y(t-l)$. a_i is the bias of the ith hidden layer.

The hidden layer output is then used to obtain the final prediction

$$\hat{y}_j(t) = f_2\left[\sum_{i=1}^{n_h} w_{ji}H_i(t) + b_j\right] \tag{6}$$

where $f_2(\cdot)$ is the output layer activation function, w_{ji} is the weight of the connection between the ith hidden neuron and the jth predicted value, b_j is the bias and n_h is the number of hidden neurons.

In this study, the input signal of the neural network is the time series of shear rate ($\dot{\gamma}(t)$) imposed in rheological measurements, and the output signal, also used as feedback, is the time series of shear
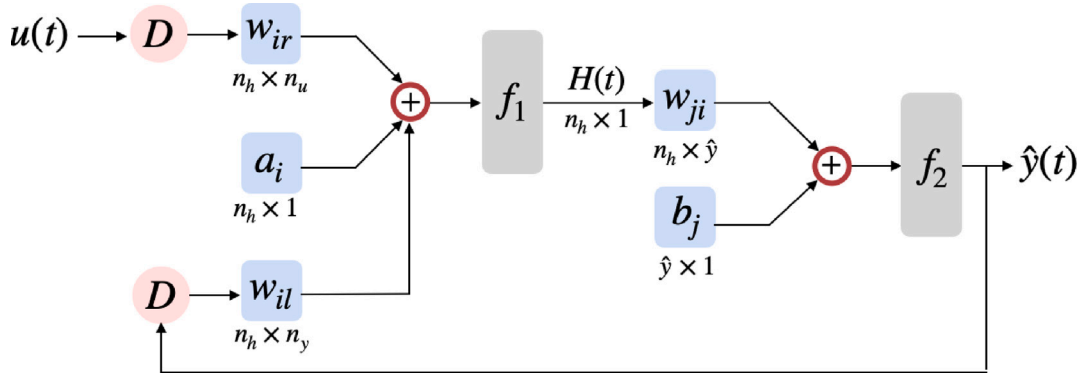
Fig. 1. NARX neural network architecture.

stress ($\sigma(t)$). The 'narxnet' function was used for constructing the neural network architecture in MATLAB. The 'tonndata' function is employed to transform the time series data into a format that is suitable for training neural networks. Selecting an appropriate training function is a pivotal decision in neural network modeling. In this study, we explored different training functions including Levenberg–Marquardt and Scaled Conjugate Gradient backpropagation. However, after careful consideration, we opted for Bayesian regularization as it demonstrated superior performance. By incorporating the previous values of both input and feedback variables, the network gains temporal context that is crucial for ensuring accurate prediction. Input and feedback delays of 1:2 were used, i.e. the neural network model takes into account the shear rates and shear stresses, respectively, in the previous two time steps to predict the shear stress response. This approach enables the neural network to leverage temporal dependencies and incorporate historical information to make more accurate predictions. The hidden layer consists of 10 neurons, which allows for a degree of complexity in the model that is capable of detecting and capturing intricate patterns in the data. The hidden layer size influences the network's predictive accuracy, which reaches steady state for hidden layer size of 10. Increasing the hidden layer size further may result in overfitting. Furthermore, we employ the open loop architecture which allows the neural network to incorporate an external input.

In order to effectively train a neural network model, a relatively large time series dataset is required that can capture the entire dynamics of the material. To this end, we trained the model with Multi Interval Thixotropic Test (MITT) experimental data, 70% of which was used for training, and 15% each for validation and testing purposes. It should be noted that special consideration was given to maintaining the temporal sequence of the samples during the partitioning process. This approach ensures that the neural network is trained using a diverse yet representative subset of the data, thereby improving its generalization capabilities.

After conducting necessary training and testing on MITT data, the neural network was subjected to input shear rate time series data from various rheological tests. The new data was formatted in a manner that aligned with the input and output requirements of the trained neural network, with the aid of the 'preparets' function. This function factors in any pre-processing steps applied during training. The trained neural network was then used to predict the shear stress based on new input shear rate data.

3. Results and discussion

As a product of bacterial culture, yogurt undergoes continuous microstructural evolution that imparts transient rheological properties to the material. This gives rise to thixotropy and influences viscoelastic and viscoplastic properties. First, we detail the training of NARX network and the fitting of SKMs to experimental MITT data (Section 3.1).

The calibrated neural network is subsequently used to predict various rheological behaviors: *(i)* thixotropy, assessed via hysteresis loop tests (Section 3.2), *(ii)* viscoelasticity, analyzed through oscillatory stress response and dynamic moduli in strain sweep tests (Section 3.3), and *(iii)* viscoplastic behavior, evaluated using steady shear viscosity and creep tests to measure yield stress and yielding dynamics (Section 3.4). SKM predictions of the rheological functions are presented for comparison in each section. Finally, we discuss the applicability of the ANN in predicting the rheology of other time dependent complex fluids in with different shear histories.

3.1. Model training/fitting with MITT

The SKMs can be analytically solved to obtain λ as a function of applied shear rate and time. The analytical solutions of SKMs I, II and III are presented in Eqs. (7)–(9) respectively.

- SKM I:

$$\lambda_{i+1} = \frac{k_2}{-k_1 \dot{\gamma}_i + k_2} + \left(\lambda_i - \frac{k_2}{-k_1 \dot{\gamma}_i + k_2} \right) e^{-\Delta t(-k_1 \dot{\gamma}_i + k_2)} \qquad (7)$$

- SKM II:

$$\lambda_{i+1} = \frac{-k_1 \lambda_i + k_2}{-k_1} e^{(-k_1 \dot{\gamma} \Delta t)} + \frac{k_2}{k_1} \qquad (8)$$

- SKM III:

$$\lambda_{i+1} = \frac{-k_1 \lambda_i \dot{\gamma} + k_2}{-k_1 \dot{\gamma}} e^{(-k_1 \dot{\gamma} \Delta t)} + \frac{k_2}{k_1 \dot{\gamma}} \qquad (9)$$

The formulation of λ takes into account the effect of shear history on the instantaneous structure of the material. The decay term in the analytical solutions of the SKMs, helps reduce the instantaneous structure λ_{i+1} as the shear rate and/or the shearing time increases. Structural breakdown caused by increasing the shearing time at a constant shear rate as well as jumping to a higher shear rate, can be captured through such a formulation. See Eq. S1 in the supplementary material for the general form of the kinetic equation used in SKMs.

Model coefficients of the SKMs were determined by minimizing the least squared error between the predicted and experimental stress response, using a custom curve fitting MATLAB code. All models considered have multiple coefficients to be determined. This makes guessing an initial value of each of these coefficients extremely difficult. It was observed that the fitting quality significantly varies with the choice of initial values of the model coefficients. Therefore, Latin Hypercube Samping (LHS) technique was used, which is a statistical tool that generates random combination of initial values within a pre-determined range. The number of samplings to be generated can be controlled, with the only bottleneck being the computational effort and time, which increases with increased number of samplings. This approach ensures
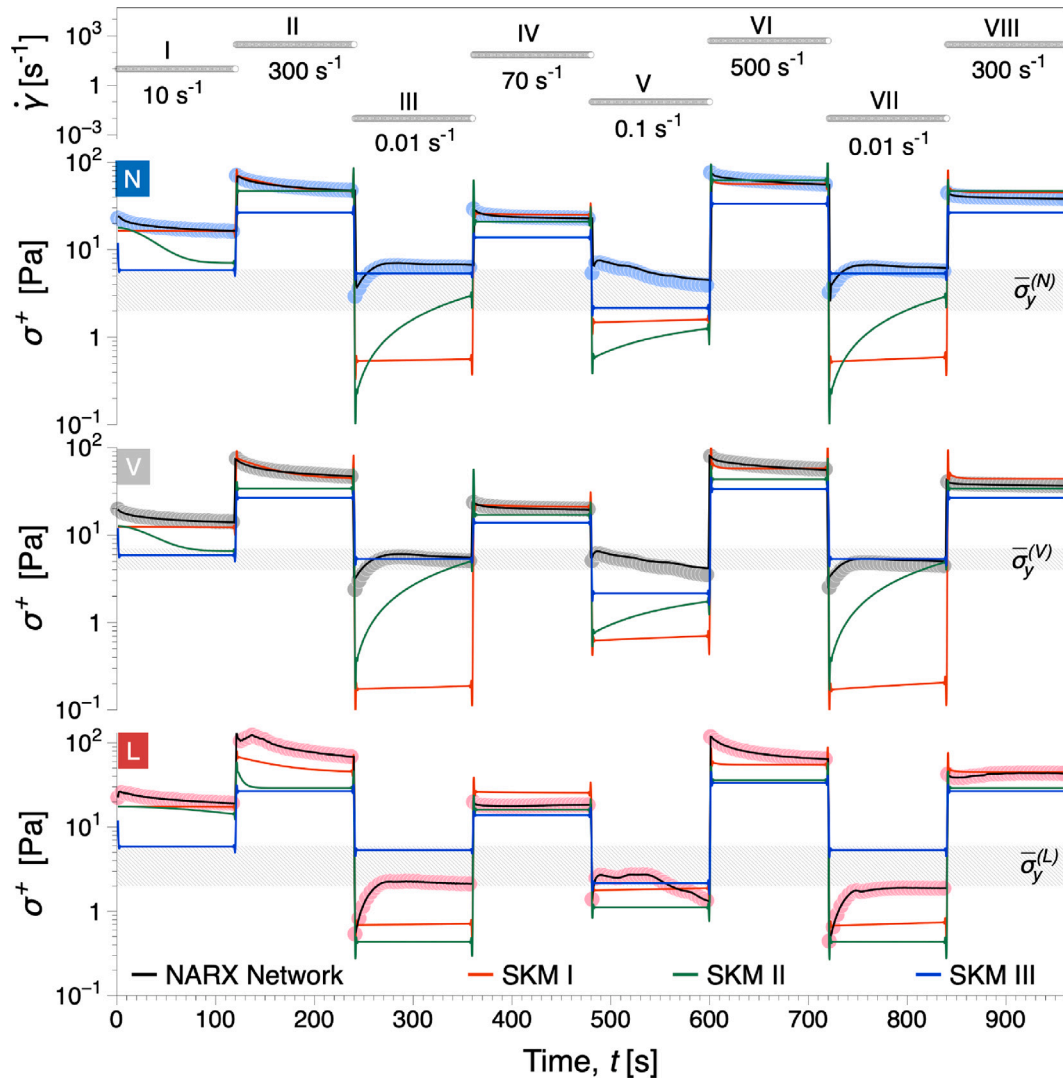
Fig. 2. Multi-Interval Thixotropic Test (MITT) results of the 3 samples. Circular symbols show the transient stress response measured in experiments and lines show the model fits. $\dot{\gamma}$ imposed in each interval is highlighted at the top of the figure.

that most initial value combinations are explored. Initial value of the structural parameter, λ_0 was chosen to be 0.5 (Fazilati et al., 2021).

Multi-interval thixotropic test (MITT) reveals the material's transient stress response to step-wise changes in shear rate, Fig. 2 (Yılmaz et al., 2016; Toker et al., 2015). MITT mimics a shear history more relevant to processing/transport applications in industries, with sudden changes in imposed shear. When the applied stress is above the yield stress, the structure breaks down and results in a decrease in transient stress response with time. For intervals I, II, IV, VI and VIII a decrease in stress can be observed, indicating structural breakdown. Whereas, when shear rates corresponding to shear stresses below the yield stress of the material are applied in intervals III, V and VII, an increase in shear stress response can be observed, indicating structural recovery. Each interval lasts 120 s. For most cases, the stress response plateaus within 120 s of the application of the shear rate. However, in certain intervals e.g. interval V, the stress first increases as a result of the structural recovery before eventually decaying with time. This fluctuation of stress occurs when the imposed shear rate corresponds to a stress in the yield stress range of the material.

The NARX neural network fits the stress response with an accuracy of 98% and captures even minor fluctuations, such as in interval V. We note that the NARX model predicts the instantaneous jump in stress at the beginning of a new interval, where the microstructural

change is maximum, with great accuracy. In comparison, the three SKMs perform poorly in predicting the stress response. While SKM I qualitatively captures the stress decay in the intervals above the yield stress range, all the SKMs fail to predict stress recovery in intervals below the yield stress. The response of material structure at different length scales to small stresses below the yield stress is highly transient and non-monotonic, which makes it difficult to capture with simple SKMs. Especially in the stress recovery intervals, the relative error in the SKM predictions is around 100%. Comparison of fitting errors in each individual interval for all the models can be found in Fig. S1 (supplementary information).

3.2. Thixotropy

Thixotropy can be quantified by calculating the hysteresis loop area in shear rate controlled steady shear test. Samples N and V exhibit similar levels of thixotropy (Fig. 3), with their hysteresis loop areas being 92.63 kPa s^{-1} and 120.61 kPa s^{-1} respectively. Sample L is much more thixotropic, with a hysteresis loop area of 235.23 kPa s^{-1}. We note that in Fig. 3, filled symbols are used to represent ramp up in shear rate and hollow symbols for ramp down. When the shear rate is ramped up, a non-linear increase in the stress can be observed (Fig. 3, left column) in the form typical of shear thinning fluids, as also seen
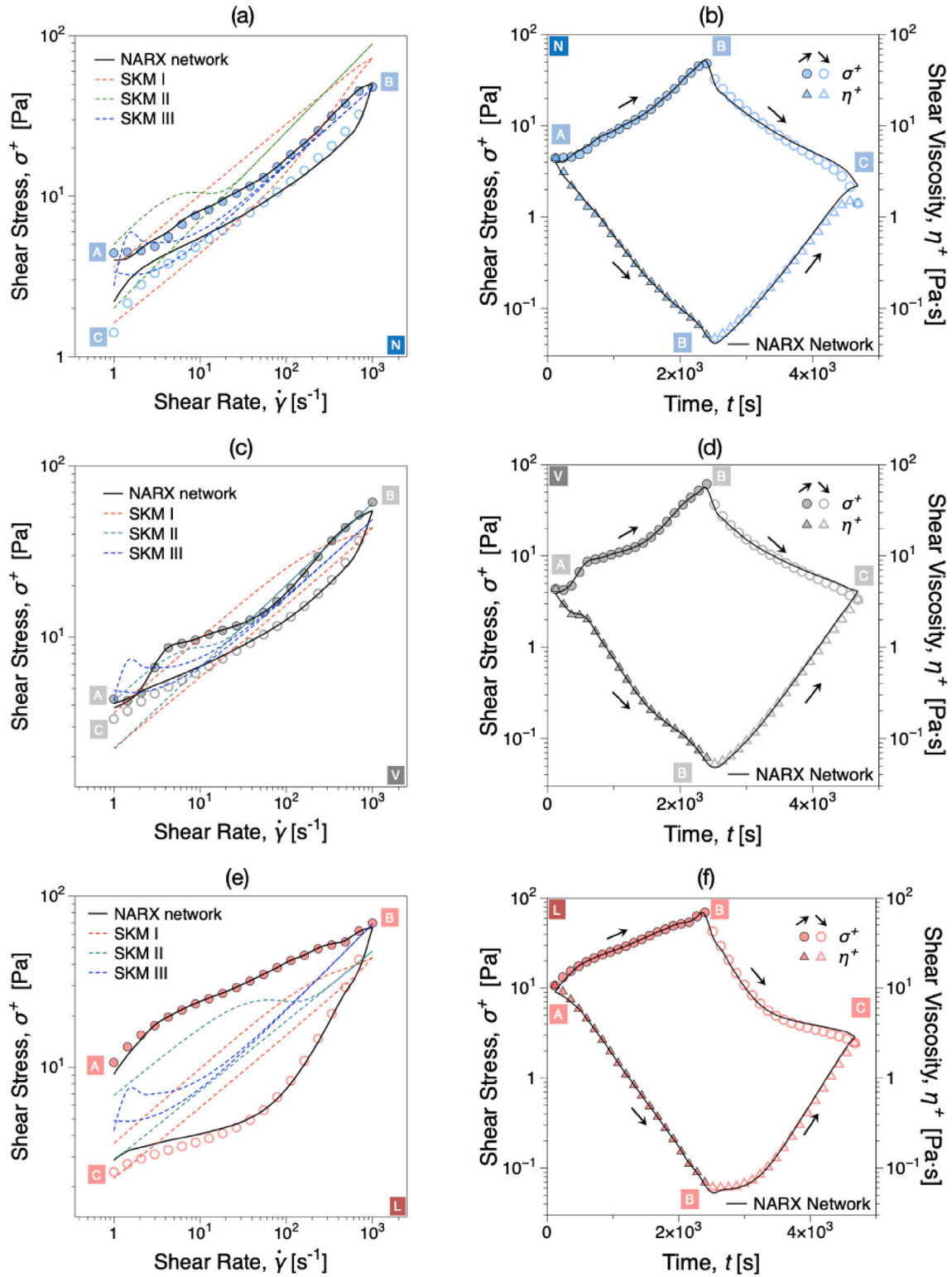
Fig. 3. Figures comparing experimental and predicted hysteresis loops, represented as (left column) shear rate dependent shear stress and (right column) time dependent stress and transient viscosity evolution: (a)–(b) N, (c)–(d) V and (e)–(f) L. Labels A,B,C correspond to the labels in Fig. 4. Black lines and colored dotted lines shows the NARX network and SKMs' predictions respectively.

in viscosity functions in Fig. 3 (right column, lower curves). During the ramp down in shear rate, the stress drops non-linearly, while recording lower values than the ramp up curve. The material undergoes more severe structural breakdown as the difference between the shear stress recorded in ramp up and down curves at a constant shear rate increases. While for N the flow curves in ramp up and down cycles do not

exhibit striking non-monotonic features, Fig. 3(a), the hysteresis loop of V shows a pronounced initial overshoot of stress at lower shear rates, $\sigma \in (2, 20)$, Fig. 3(c). The stress overshoot is caused due to the breakdown of initial structure after startup, dominating the time evolution of stress (Mewis and Wagner, 2009), and also due to elastic effects (Serial et al., 2021). At high shear rates, the overshoot levels off
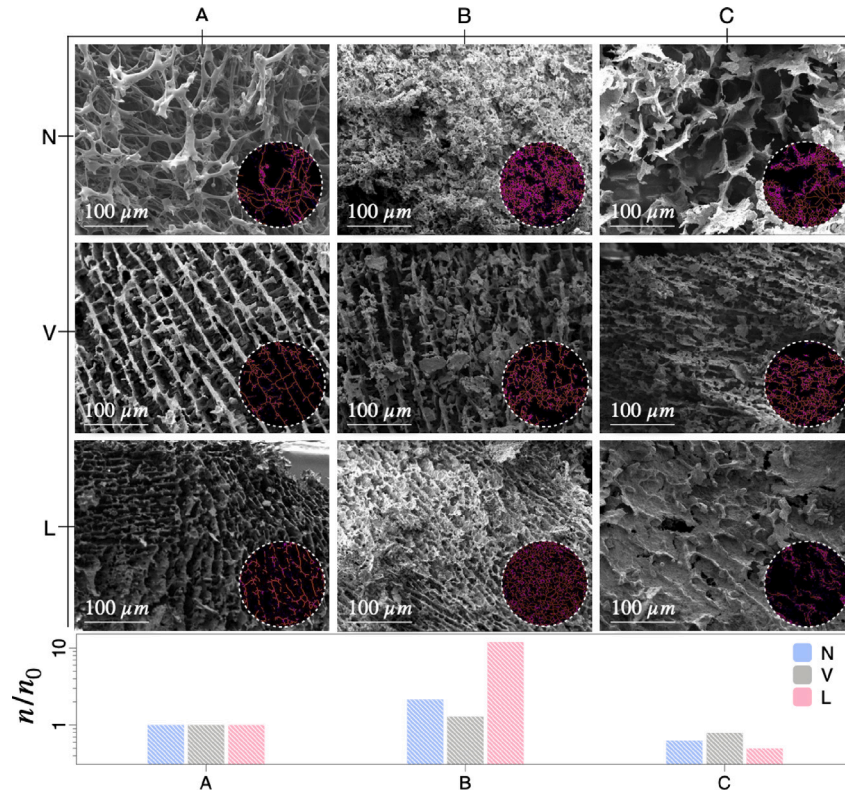
Fig. 4. SEM micrographs for N, V and L yogurt samples, captured at different shear levels in a hysteresis loop test. A: Unsheared sample, B: Sample sheared by ramp up from 10^0–10^3 s^{-1}, C: Sample obtained after completion of hysteresis loop tests.

and stresses close to sample N were recorded. In contrast to both N and V, a relatively large thixotropic loop was obtained for sample L. Stresses at the end of the measurement are almost 8 Pa lower than the initial stress level, suggesting more severe structural breakdown compared to N and V, which show a drop of 2–4 Pa in the end. Factors influencing the recovery of L include increased fat content that impede structural network recovery, and increased bacterial activity resulting from the two bacterial cultures used.

Results of numerical modeling comparing the hysteresis loop predictions of the NARX neural network and the SKMs are summarized in Fig. 3 (left column). The fitted model parameters of the SKMs can be found in Table S2 in supplementary information. The neural network predicts the thixotropic behavior in hysteresis loop test with an average relative error of 8%. However, for most shear rates the error is less than 2%, and the prediction suffers only towards the end of the test as the input regressor gets filled with estimated values of the time series. In comparison, only SKM I can capture the overall shape of the hysteresis loop for samples N and V, albeit having much higher prediction errors of around 74%. Both SKMs II and III qualitatively predict a stress overshoot at low shear rates, as observed in sample V. However, they fall short in magnitude. In the case of sample L, where structural breakdown dominates due to higher thixotropy, the SKMs completely fail to predict the transient stress response of the material. Moreover, the superior predictive capabilities of the NARX model is highlighted when the non-monotonic stress response is plotted as a time series in Fig. 3 (right column). A comparison between NARX and SKM prediction errors can be found in Fig. S2, supplementary information.

We briefly emphasize the effectiveness of the ANN in capturing thixotropic effects by a microstructural analysis highlighting the transient structural evolution. The microstructure of thixotropic materials evolves with time and shear rate, influencing stress response and introducing shear history dependence. Microstructural changes due to thixotropy were analyzed at three shear history levels during hysteresis

loop tests. For each yogurt sample, SEM images were taken of unsheared samples (points A in Fig. 3), samples sheared from $\dot{\gamma} = 10^0$–10^3 s^{-1} (points B in Fig. 3), and samples after completing a full hysteresis cycle (points C in Fig. 3). Image analysis was performed to quantify structural interconnectivity by calculating the number of structural branches (Fig. 4, circular insets). Unsheared samples displayed an intricate protein and casein network (Fig. 4(A)). Shearing increased the number of branches by 100%, 120%, and 1000% for samples N, V, and L respectively. At the end of the hysteresis test, branch counts decreased as the structure partially recovered, forming larger branches from smaller ones, reducing branch numbers to 63%, 80%, and 50% of the initial counts for samples N, V, and L, respectively. The structure did not fully recover to its original state due to thixotropic effects, explaining the shear stress drop at the end of the hysteresis loop test (Fig. 3(a)–(c)).

3.3. Viscoelasticity

In order to predict oscillatory shear data, which is commonly plotted as storage (G') and loss (G'') moduli vs. the shear strain amplitude (γ_0), we must consider the underlying time-dependant imposed strain ($\gamma(t)$) and resulting time-dependent stress ($\sigma(t)$). For a sinusoidal shear strain input, $\gamma(t) = \gamma_0 \sin(\omega t)$, the resulting time dependent shear stress in a linear viscoelastic oscillatory shear test is $\sigma(t) = \sigma_0 \sin(\omega t + \delta)$, where δ is the phase angle. The storage and loss moduli are defined as $G' = \sigma_0/\gamma_0 \cos \delta$ and $G'' = \sigma_0/\gamma_0 \sin \delta$, respectively. The intracycle material response has gained significant attention particularly in the nonlinear regime, where the sinusoidal strain input results in a non-sinusoidal stress output, i.e. nonlinear material response (Hyun et al., 2011; Kamkar et al., 2022). The time-dependent data is represented in Fig. 5 in the form of elastic and viscous Lissajous–Bowditch (LB) diagrams.

The tested samples exhibit similar viscoelastic characteristics with a pronounced gel-like behavior ($G' > G''$) and equal loss factor,
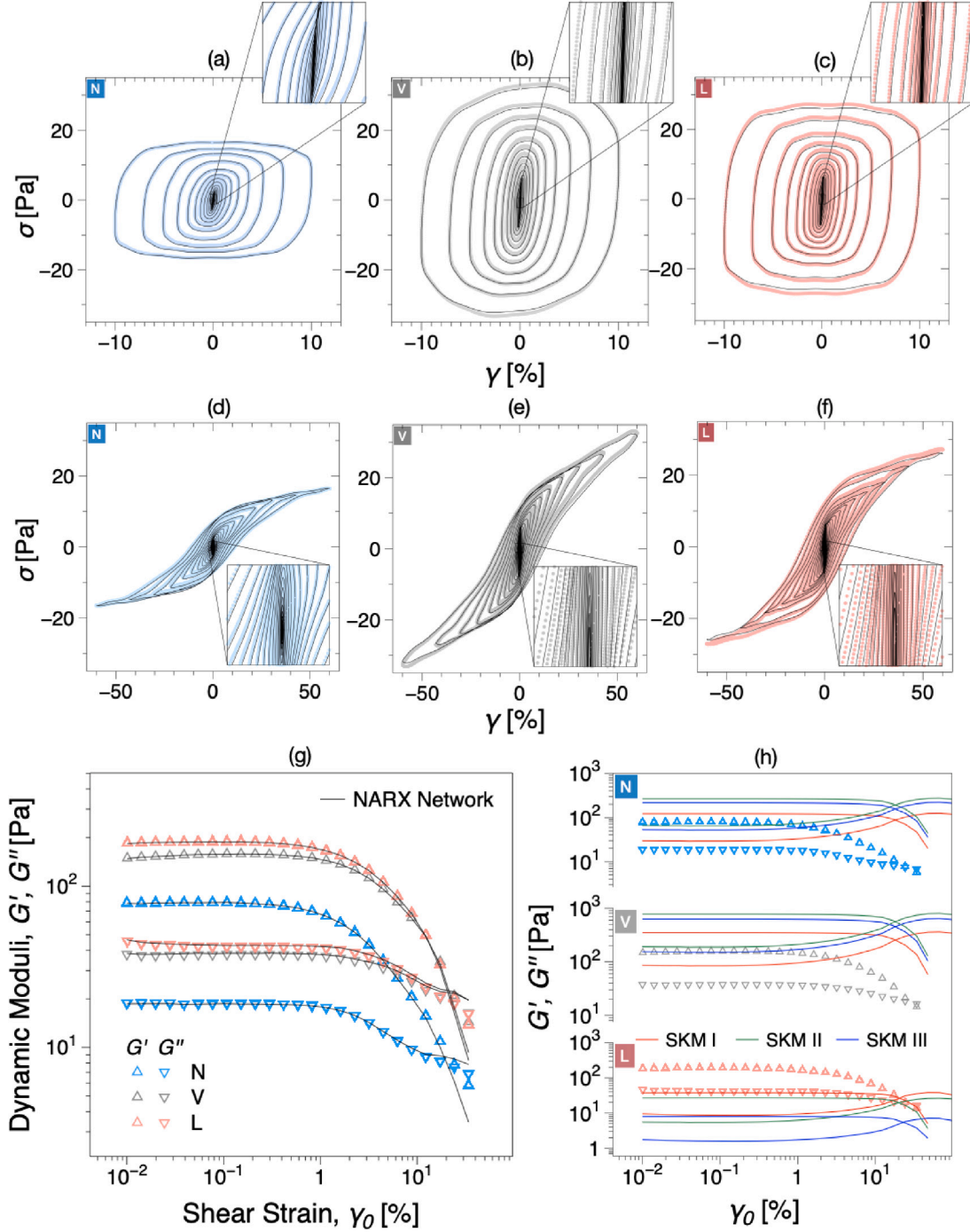
Fig. 5. Elastic ((a)–(c)) and Viscous ((d)–(f)) Lissajous-Bowditch (LB) plots showing the time dependent intra-cycle stress $\sigma(t)$ as function of the time-dependent shear strain $\gamma(t)$ and $\sigma(t)$ as function of the time-dependent shear rate $\dot{\gamma}(t)$ for all strain amplitudes investigated at $\omega = 6$ rad/s. (g) Oscillatory shear strain amplitude (γ_0) sweep test showing the linear viscoelastic storage, G' and loss G'' moduli as function of the shear strain amplitude, γ_0 performed at $\omega = 6$ rad/s. Note that each data point in the plot corresponds to one loop in the LB plots. In all figures, triangular symbols and black lines represent experiments and NARX network predictions respectively. (h) SKM prediction of dynamic moduli in strain sweep test.

$\tan \delta \sim 0.23$, while samples V and L record higher magnitudes of G' and G'' compared to N (Fig. 5(g)). Time series of shear rate obtained from the imposed strain is used as an input to the neural network to obtain shear stress predictions. NARX network (black lines in Fig. 5) accurately captures intra-cycle nonlinear behavior in both linear and nonlinear viscoelastic loops, as well as the dynamic moduli evolution in strain sweep test. This effectively means that a full nonlinear data analysis could be performed using the predicted NARX data. For the

sake of brevity, here we focus on the linear viscoelastic dynamic moduli. Thus, in comparison, the SKMs can only predict the loss factor accurately while missing the dynamic moduli magnitudes in strain sweep tests and slightly overestimating the linear viscoelastic range (LVR), Fig. 5(h). SKM prediction of G'' curves show an overshoot post $G' - G''$ crossover, a characteristic feature of several gels showing weak strain overshoot (Amini et al., 2024). It is important to note that the analytical solutions of the chosen common SKMs do not contain a term
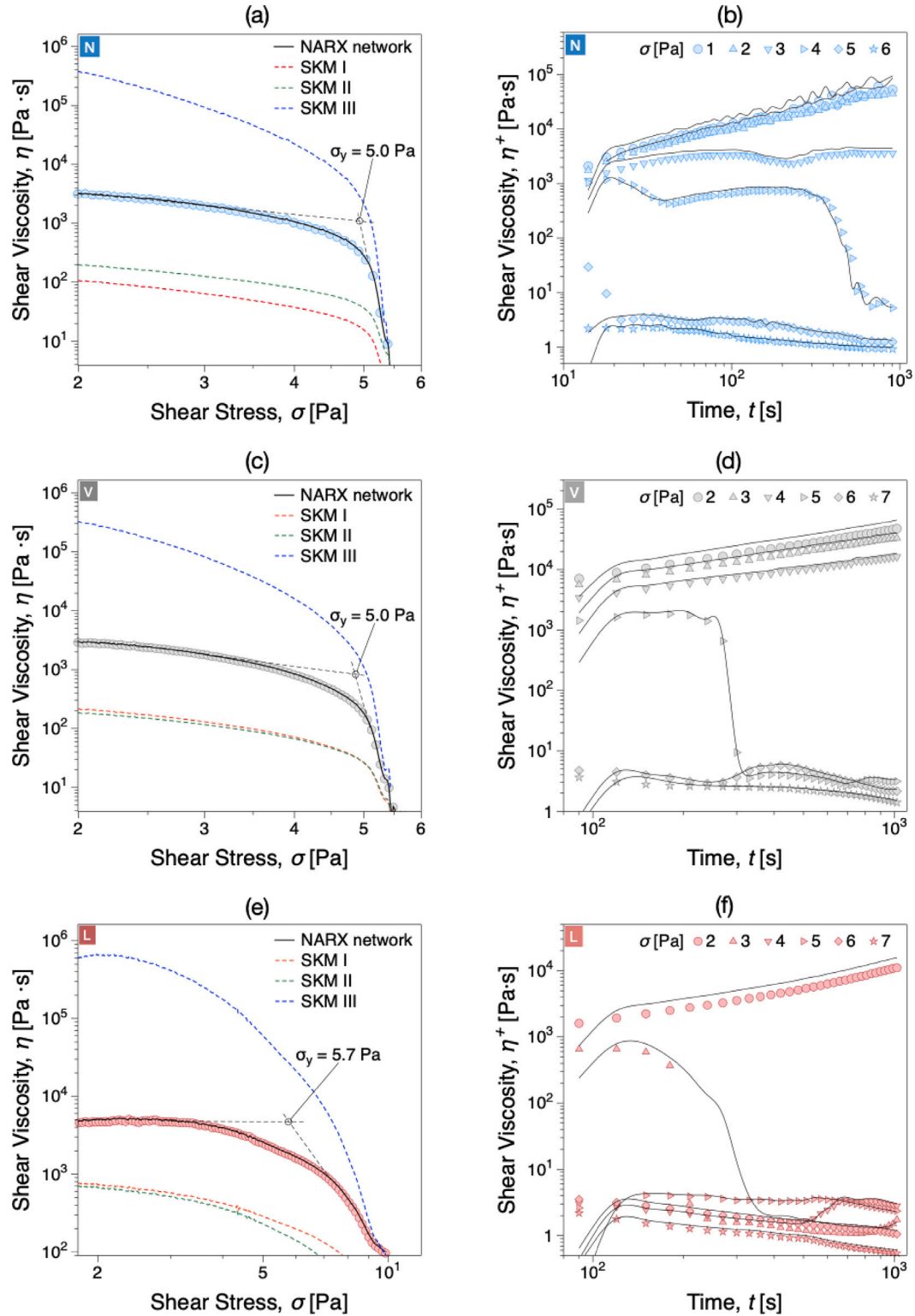
Fig. 6. Comparison between steady shear stress viscosity functions (left column) and creep tests when estimating the yield stress range (right column): (a)–(b) N, (c)–(d) V and (e)–(f) L.

accounting for viscoelasticity explicitly. However, the equation of state considers the onset of yielding through a power law term at low shear rates, which explains the ability of the SKMs to qualitatively capture the departure from LVR. A comparison between NARX and SKM prediction errors can be found in Fig. S3, supplementary information.

3.4. Viscoplasticity

Yield stress obtained from shear stress-controlled viscosity tests for the three yogurt samples are presented in Fig. 6(a), (c) and (e). Samples N and V have equal yield stresses ($\sigma_y^{(N)}, \sigma_y^{(V)} = 5.0$ Pa), whereas sample L shows a 14% increase ($\sigma_y^{(L)} = 5.7$ Pa). This approach of measuring
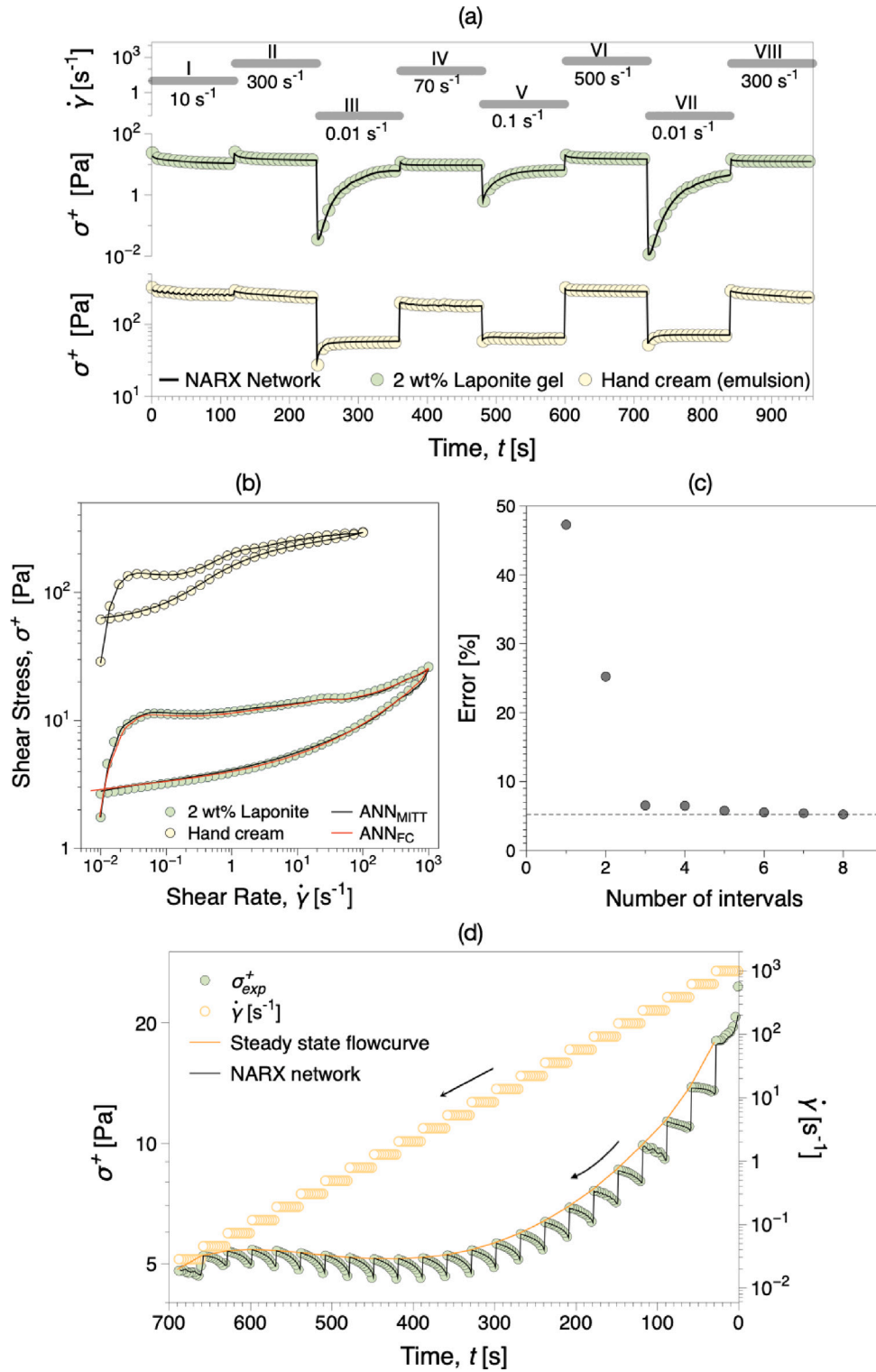
Fig. 7. (a) MITT training and (b) hysteresis loop predictions of the ANN for Laponite and hand cream samples. (c) Error in ANN's prediction of Laponite's thixotropy in hysteresis loop test, trained on increasing number of MITT intervals. (d) Transient stress response to a decreasing shear rate ramp. The orange curve shows the steady state stress (flow curve) of Laponite 2 wt%, while the black curve shows the ANN. ANN trained on the transient flow curve data predicts the hysteresis loop with 95.8% accuracy, Fig. 7(b) red curve.

yield stress assumes the existence of a single critical stress above which the material yields. In reality, most yield stress fluids exhibit a gradual transition from elastic to plastic deformation (Møller et al., 2006). This gradual transition necessitates the existence of a range of stresses in which the material yields. This is further confirmed as the viscosity curves do not show a sharp drop in Fig. 6(a), (c) and (e). Therefore,

creep tests were performed where the time evolution of viscosity is recorded at different constant imposed stresses (Fig. 6(b), (d) and (e)). A new sample was used for every imposed shear stress to ensure that shear history does not affect the measurements. The measured yield stress ranges of the three samples are as follows; $\sigma_y^{(N)} \in (2, 6)$ Pa, $\sigma_y^{(V)} \in (4, 7)$ Pa and $\sigma_y^{(L)} \in (2, 6)$ Pa.

Apart from revealing the transient material behavior, creep tests also give an estimate of the time required to achieve steady state. Extended tests were therefore performed (data not shown) and an apparent steady state could be reached after 2000 s of shearing for most but not all shear rates. This is an effect of thixotropy that makes it difficult for the structure to achieve steady state. It is interesting to note that while stress controlled viscosity tests (Fig. 6(a) and (c)) suggest that samples N and V have equal yield stresses, creep tests (Fig. 6(b) and (d)) reveal that sample V yields at a slightly higher stress range compared to N. In other words, higher stresses are required to transition from elastic to plastic deformation. This dominance of elastic forces prior to yielding causes a more dramatic stress overshoot at the lowest shear rates in the beginning of the hysteresis loop for sample V (Fig. 3(c)).

Model predictions are also shown in Fig. 6. In stress-controlled viscosity tests, NARX neural network not only perfectly captures the yield stress value but also the transient state prior to yielding with errors less than 1%, Fig. 6(a), (c) and (e). SKMs I and II underestimate and SKM III overestimates the viscosity function by thousands of Pascals. However, for samples N and V, SKMs can predict the magnitude of yield stress (stress when the viscosity drops) in stress controlled viscosity tests with good accuracy. This is a result of the formulation of the equation of state (Table 1), where the first term acts as yield stress prior to yielding, at lower shear rates ($\dot{\gamma} \ll \dot{\gamma}_y$). It is interesting to note that the NARX network can also predict highly transient breakdown and buildup of material structure in creep tests (Fig. 6(b), (d) and (f)), while also capturing the viscosity fluctuation when the imposed stress is in the yield stress range. Understandably, the prediction slightly suffers for stresses below the yield stress range as elastic forces dominate. However, as the imposed stress increases and the material transitions towards plastic deformation, the predictions become more accurate. For the sake of clarity, only the neural network's predictions of the creep curves are shown as the SKMs fail to capture the viscosity magnitude in stress controlled viscosity tests, (Fig. 6, left column). A comparison between NARX and SKM prediction errors can be found in Fig. S4, supplementary information.

3.5. Discussion

The ANN demonstrates a high level of accuracy in capturing the transient rheological behavior of yogurt. To assess the generalizability of the ANN in predicting transient rheological properties across various material types, we examined Laponite gel and hand cream, both of which are categorized as thixo-elasto-viscoplastic (TEVP) fluids. Laponite is a widely utilized polymer known for its role as a rheology modifier and emulsion stabilizer in a diverse range of products, including household cleaning agents, personal care items, agricultural formulations, and pharmaceutical applications. In contrast, hand cream is an emulsion characterized by its complex rheological behavior, exhibiting high yield stress along with thixotropic and viscoelastic properties.

A 2 wt% Laponite (Conservation Resources, UK) suspension was prepared by dispersing the polymer in deionized water, followed by homogenization with an overhead mixer at 2000 RPM for 30 min. The crosslinking results in an increase of viscosity as the material transitions to gel. It takes up to three days for Laponite to become stable and attain a steady state rheology.

The ANN was trained on MITT performed on Laponite and hand cream samples (Fig. 7(a)), following the measurement methodology previously discussed for yogurt. The ANN learns the time dependent behavior with minimal training errors of 2.3% for Laponite and 2.9% for hand cream. Once trained, the ANN was employed to predict the transient stress response in hysteresis loop tests, achieving remarkable prediction accuracies of 95% for Laponite and 97.5% for hand cream, Fig. 7(b). Hysteresis loop tests were performed on different range of shear rates, specifically $\dot{\gamma} \in [10^{-2}, 10^{3}]$ s^{-1} for Laponite and $\dot{\gamma} \in [10^{-2}, 10^{2}]$ s^{-1} for hand cream, to evaluate the ANN's predictability

of different shear histories. The performance of any ANN is highly dependent upon the quality and quantity of training data utilized. In our investigation, we explored the optimal number of MITT intervals required to achieve effective network training for reliable predictions. Remarkably, our findings revealed that only four intervals, which equates to 480 s of transient data, were sufficient to achieve the optimal prediction accuracy for Laponite, Fig. 7(c). Therefore, eight intervals with a broad range of shear rates were employed in this study to capture both structural breakdown and recovery.

Furthermore, we assessed the ANN's performance when trained on a different rheological test that involved varying shear history. Specifically, the material's stress response to a decreasing shear rate ramp was evaluated, Fig. 7(d). The steady-state flow curve contains critical information about the material's rheology and is often employed to extract coefficients of shear-thinning and viscoplastic constitutive models through curve fitting. The transient stress response was measured at each imposed shear rate for 30 s (data acquisition at 1 point/s), sufficient time for the stress to reach an apparent steady state. The steady state stress at each imposed shear rate was extracted to construct the flow curve of the material. The trained network predicts the thixotropic behavior in hysteresis loop with an accuracy of 95.8%, highlighting the ANN's remarkable flexibility and adaptability in processing various types of transient rheological data.

4. Conclusions

Complex fluids exhibit transient non-monotonic rheological properties which are difficult to model, specially for materials with evolving microstructure. In this study we show that a NARX neural network can predict the thixo-elasto-viscoplastic (TEVP) rheological properties of yogurt using a data driven approach, without the need of constitutive equations. By training the network to stress response in a simple rate controlled test (MITT) the NARX model identifies intricate patterns in material functions and their dependence on the shear history, as the model considers the shear stress response in the past two time steps for prediction. The trained NARX model can accurately predict thixotropy in hysteresis loop tests with 92% accuracy, viscoelasticity in oscillatory tests and viscoplasticity in stress controlled viscosity and creep tests with an accuracy of more than 98%. For comparison, SKMs are fitted to MITT to determine model parameters and the complete model is then used to predict TEVP behavior in the same tests. It is evident that the SKMs fail to capture the intricate dependence of the shear stress/viscosity response to the shear history and show prediction errors of greater than 100% in most cases. The flexibility of the ANN to predict rheology was demonstrated by predicting the stress response of Laponite and hand cream with 95% and 97.5% accuracy respectively. Additionally, the ANN shows similar performance when trained on a different transient test. With the evolution of artificial intelligence technologies, ANN can be used to digitally characterize rheology of complex fluids and shows potential to complement and even replace tedious rheological characterization.

CRediT authorship contribution statement

Ases Akas Mishra: Writing – original draft, Visualization, Validation, Software, Methodology, Investigation, Formal analysis, Conceptualization. **Viney Ghai:** Visualization. **Valentina Matovic:** Writing – original draft, Investigation, Data curation. **Dragana Arlov:** Writing – review & editing, Resources, Methodology, Funding acquisition. **Roland Kádár:** Writing – review & editing, Resources, Methodology, Funding acquisition.

Declaration of competing interest

The authors declare that they have no known competing financial interests or personal relationships that could have appeared to influence the work reported in this paper.

Acknowledgments

Appendix A. Supplementary data

Supplementary material related to this article can be found online at https://doi.org/10.1016/j.engappai.2024.109598.

Data availability

Data will be made available on request.

References

Abdelsalam, S.I., Abdelwahab, E.T., Eldesoky, I., Abumandour, R.M., Ahmed, M., 2025. Benchmarking the composite performance of distinct shapes of ferrometallic gold nanoshells: photothermal cancer therapy. Acta Mech. Sin. 41 (6), 1–13.

Abdelsalam, S.I., Alsedais, N., Aly, A.M., 2024a. Revolutionizing bioconvection: Artificial intelligence-powered nano-encapsulation with oxytactic microorganisms. Eng. Appl. Artif. Intell. 137, 109128.

Abdelsalam, S.I., Magesh, A., Tamizharasi, P., 2024b. Optimizing fluid dynamics: An in-depth study for nano-biomedical applications with a heat source. J. Therm. Anal. Calorim. 1–13.

Abu-Jdayil, B., Mohameed, H., 2002. Experimental and modelling studies of the flow properties of concentrated yogurt as affected by the storage time. J. Food Eng. 52 (4), 359–365.

Amini, K., Mishra, A.A., Sivakumar, A.K., Arlov, D., Innings, F., Kádár, R., Tammisola, O., Lundell, F., 2024. Scaling laws for near-wall flows of thixo-elasto-viscoplastic fluids in a millifluidic channel. Phys. Fluids 36 (2).

Barnes, H.A., 1997. Thixotropy—a review. J. Non-Newton. Fluid Mech. 70 (1–2), 1–33.

Bauer, W., Collins, E., 1967. In: Eirich, F.R. (Ed.), Rheology, vol. 4, Academic Press, New York and London, (Chapter 8).

Bénézech, T., Maingonnat, J.F., 1993. Flow properties of stirred yoghurt: structural parameter approach in describing time-dependency. J. Texture Stud. 24 (4), 455–473.

Benezech, T., Maingonnat, J.F., 1994. Characterization of the rheological properties of yoghurt—a review. J. Food Eng. 21 (4), 447–472.

Bhattacharyya, T., Jacob, A.R., Petekidis, G., Joshi, Y.M., 2023. On the nature of flow curve and categorization of thixotropic yield stress materials. J. Rheol. 67 (2), 461–477.

Boosjin, S.N., Noghani, V.F., Hashemiravan, M., 2016. Characterization of probiotic fermented milk prepared by different inoculation size of mesophilic and thermophilic lactic acid bacteria. Appl. Food Biotechnol. 3 (4), 276–282.

Chen, C., Zhao, S., Hao, G., Yu, H., Tian, H., Zhao, G., 2017. Role of lactic acid bacteria on the yogurt flavour: A review. Int. J. Food Prop. 20 (sup1), S316–S330.

Choi, J., Armstrong, M., Rogers, S.A., 2021. The role of elasticity in thixotropy: Transient elastic stress during stepwise reduction in shear rate. Phys. Fluids 33 (3), 033112.

Coussot, P., Nguyen, Q.D., Huynh, H., Bonn, D., 2002a. Avalanche behavior in yield stress fluids. Phys. Rev. Lett. 88 (17), 175501.

Coussot, P., Nguyen, Q.D., Huynh, H., Bonn, D., 2002b. Viscosity bifurcation in thixotropic, yielding fluids. J. Rheol. 46 (3), 573–589.

Dimitriou, C.J., McKinley, G.H., 2014. A comprehensive constitutive law for waxy crude oil: a thixotropic yield stress fluid. Soft Matter 10 (35), 6619–6644.

Dullaert, K., Mewis, J., 2006. A structural kinetics model for thixotropy. J. Non-Newton. Fluid Mech. 139 (1–2), 21–30.

Fazilati, M., Ingelsten, S., Wojno, S., Nypelö, T., Kádár, R., 2021. Thixotropy of cellulose nanocrystal suspensions. J. Rheol. 65 (5), 1035–1052.

Ghania, E., Abdelsalam, S.I., Megahed, A., Hosni, A., Zaher, A., 2024. Computational workflow to monitor the electroosmosis of nanofluidic flow in the vicinity of a bounding surface. Numer. Heat Transfer B 1–15.

Hyun, K., Wilhelm, M., Klein, C.O., Cho, K.S., Nam, J.G., Ahn, K.H., Lee, S.J., Ewoldt, R.H., McKinley, G.H., 2011. A review of nonlinear oscillatory shear tests: Analysis and application of large amplitude oscillatory shear (LAOS). Prog. Polym. Sci. 36 (12), 1697–1753.

Kamkar, M., Salehiyan, R., Goudoulas, T.B., Abbasi, M., Saengow, C., Erfanian, E., Sadeghi, S., Natale, G., Rogers, S.A., Giacomin, A.J., et al., 2022. Large amplitude oscillatory shear flow: Microstructural assessment of polymeric systems. Prog. Polym. Sci. 132, 101580.

Larson, R.G., Wei, Y., 2019. A review of thixotropy and its rheological modeling. J. Rheol. 63 (3), 477–501.

Lee, T.-C., Kashyap, R.L., Chu, C.-N., 1994. Building skeleton models via 3-D medial surface axis thinning algorithms. CVGIP, Graph. Models Image Process. 56 (6), 462–478.

Lin, T., Horne, B.G., Giles, C.L., 1998. How embedded memory in recurrent neural network architectures helps learning long-term temporal dependencies. Neural Netw. 11 (5), 861–868.

Mahmoudabadbozchelou, M., Jamali, S., 2021. Rheology-informed neural networks (RhINNs) for forward and inverse metamodeling of complex fluids. Sci. Rep. 11 (1), 12015.

Mahmoudabadbozchelou, M., Kamani, K.M., Rogers, S.A., Jamali, S., 2022. Digital rheometer twins: Learning the hidden rheology of complex fluids through rheology-informed graph neural networks. Proc. Natl. Acad. Sci. 119 (20), e2202234119.

Mahmoudabadbozchelou, M., Kamani, K.M., Rogers, S.A., Jamali, S., 2024. Unbiased construction of constitutive relations for soft materials from experiments via rheology-informed neural networks. Proc. Natl. Acad. Sci. 121 (2), e2313658121.

Menezes, Jr., J.M.P., Barreto, G.A., 2008. Long-term time series prediction with the NARX network: An empirical evaluation. Neurocomputing 71 (16–18), 3335–3343.

Mewis, J., Wagner, N.J., 2009. Thixotropy. Adv. Colloid Interface Sci. 147, 214–227.

Mishra, A.A., Momin, A., Strano, M., Rane, K., 2022. Implementation of viscosity and density models for improved numerical analysis of melt flow dynamics in the nozzle during extrusion-based additive manufacturing. Prog. Addit. Manuf. 1–14.

Møller, P.C., Mewis, J., Bonn, D., 2006. Yield stress and thixotropy: on the difficulty of measuring yield stresses in practice. Soft Matter 2 (4), 274–283.

Mujumdar, A., Beris, A.N., Metzner, A.B., 2002. Transient phenomena in thixotropic systems. J. Non-Newton. Fluid Mech. 102 (2), 157–178.

Nagrani, P.P., Kulkarni, R.V., Kelkar, P.U., Corder, R.D., Erk, K.A., Marconnet, A.M., Christov, I.C., 2023. Data-driven rheological characterization of stress buildup and relaxation in thermal greases. J. Rheol. 67 (6), 1129–1140.

Nijenhuis, K., McKinley, G.H., Spiegelberg, S., Barnes, H.A., Aksel, N., Heymann, L., Odell, J.A., 2007. Springer Handbook of Experimental Fluid Mechanics. Springer, pp. 619–732, (Chapter 9. Non-Newtonian Flows).

Pearlmutter, B.A., 1995. Gradient calculations for dynamic recurrent neural networks: A survey. IEEE Trans. Neural Netw. 6 (5), 1212–1228.

Pinder, K.L., 1964. Time dependent rheology of the tetrahydrofuran-hydrogen sulphide gas hydrate slurry. Can. J. Chem. Eng. 42 (3), 132–138.

Prajapati, D.M., Shrigod, N.M., Prajapati, R.J., Pandit, P.D., 2016. Textural and rheological properties of yoghurt: a review. Adv. Life Sci. 5 (13), 5238–5254.

Ramaswamy, H., Basak, S., 1991. Rheology of stirred yogurts. J. Texture Stud. 22 (2), 231–241.

Salehi, S., Arashpour, M., Golafshani, E.M., Kodikara, J., 2023. Prediction of rheological properties and ageing performance of recycled plastic modified bitumen using machine learning models. Constr. Build. Mater. 401, 132728.

Schindelin, J., Arganda-Carreras, I., Frise, E., Kaynig, V., Longair, M., Pietzsch, T., Preibisch, S., Rueden, C., Saalfeld, S., Schmid, B., et al., 2012. Fiji: an open-source platform for biological-image analysis. Nat. Methods 9 (7), 676–682.

Serial, M.R., Bonn, D., Huppertz, T., Dijksman, J.A., van der Gucht, J., Van Duynhoven, J.P., Terenzi, C., 2021. Nonlocal effects in the shear banding of a thixotropic yield stress fluid. Phys. Rev. Fluids 6 (11), 113301.

Taherdoost, H., 2023. Deep learning and neural networks: Decision-making implications. Symmetry 15 (9), 1723.

Toker, O.S., Karasu, S., Yilmaz, M.T., Karaman, S., 2015. Three interval thixotropy test (3ITT) in food applications: A novel technique to determine structural regeneration of mayonnaise under different shear conditions. Food Res. Int. 70, 125–133.

Toorman, E.A., 1997. Modelling the thixotropic behaviour of dense cohesive sediment suspensions. Rheol. Acta 36 (1), 56–65.

Tucker, G., 2017. Applications of rheological data into the food industry. In: Advances in Food Rheology and its Applications. Elsevier, pp. 159–175.

Wei, Y., Solomon, M.J., Larson, R.G., 2018. A multimode structural kinetics constitutive equation for the transient rheology of thixotropic elasto-viscoplastic fluids. J. Rheol. 62 (1), 321–342.

Worrall, W., Tuliani, S., 1964. Viscosity changes during the ageing of clay-water suspensions. Trans. J. Br. Ceram. Soc. 63, 167–185.

Yılmaz, M.T., Kutlu, G., Tulukcu, E., Toker, O.S., Sagdic, O., Karaman, S., 2016. Rheological characteristics of salvia sclarea seed gum solutions at different hydration temperature levels: Application of three interval thixotropy test (3ITT). LWT-Food Sci. Technol. 71, 391–399.

Zhang, T., Wang, D., Lu, Y., 2023. RheologyNet: A physics-informed neural network solution to evaluate the thixotropic properties of cementitious materials. Cem. Concr. Res. 168, 107157.